Reinvestigating group-velocity-tunable Bessel-X optical wave-packets

Zhaoyang Li (lizy@zjlab.ac.cn)
Shanghai Zhangjiang Laboratory
Yanqi Liu
Shanghai Institute of Optics and Fine Mechanics
Yuxin Leng
Shanghai Institute of Optics and Fine Mechanics
Ruxin Li
Shanghai Institute of Optics and Fine Mechanics

Research Article

Keywords:

Posted Date: April 14th, 2022

DOI: https://doi.org/10.21203/rs.3.rs-1551367/v1

Reinvestigating group-velocity-tunable Bessel-X optical wave-packets

Zhaoyang Li[1,2✉], Yanqi Liu[3], Yuxin Leng[3] & Ruxin Li[1,3,4]

[1]Zhangjiang Laboratory, 100 Haike Road, Pudong, Shanghai 201210, China
[2]Institute of Laser Engineering, Osaka University, 2-6 Yamada-oka, Suita, Osaka 565-0871, Japan
[3]Shanghai Institute of Optics and Fine Mechanics, Chinese Academy of Sciences, 390 Qinghe Road, Jiading, Shanghai 201800, China
[4]ShanghaiTech University, 393 Middle Huaxia Road, Pudong, Shanghai 201210, China
✉email: lizy@zjlab.ac.cn

Abstract
The group-velocity of the Bessel-X optical wave-packet can be controlled by introducing well-designed arbitrarily-axisymmetric pulse-front deformation, which permits realizing superluminal, subluminal, accelerating, decelerating, and even nearly-programmable group-velocities. To better understand the tunability of the group-velocity, the generation methods of this Bessel-X optical wave-packet and the mechanisms of the tunable group-velocity in both the physical and the Fourier spaces are investigated. We also studied the relationship with the recently-reported space-time optical wave-packet, and the group-velocity-tunable Bessel-X optical wave-packet is a subsection of the space-time optical wave-packet.

Introduction
Controlling the group-velocity of an optical pulse, especially a propagation-invariant optical wave-packet, is an interesting and important research, which has many unique applications from optics to physics and engineering [1-6]. The Bessel beam is a very famous family of propagation-invariant beams [7, 8], which nearly does not spread out in space during very-long-distance propagation much exceeding the Rayleigh length [9, 10]. Apart from the propagation-invariance, the Bessel beam, compared with the Gaussian beam, has many other unique characteristics like self-healing, superluminal (both phase and group velocities), etc. [11-13], which further enhance its unique applications [14]. A monochromatic Bessel beam is propagation-invariant in space, while a broadband Bessel wave-packet can maintain its invariant intensity profile in both space and time, which accordingly becomes a very important family of propagation-invariant wave-packets [15-17]. The previous researches show the Bessel wave-packet can be expressed as a coherent conical superposition of monochromatic Bessel beams of a range of frequencies. Because the Bessel wave-packet, firstly studied in acoustics, has a letter "*X*" like spatiotemporal distribution and is consequently named as the X-wave [15, 16], its optical version is then named as the Bessel-X beam [17]. Some other forms of the Bessel optical wave-packet such as focus wave modes [18-21], light-needles [22], or light-bullets [23], etc. can be produced by modulating angular/spatial dispersion (frequency-dependent conical angles), polarization, or temporal dispersion, etc. in the coherent conical superposition of monochromatic Bessel beams with different frequencies. These Bessel optical wave-packets further enhance the unique characteristics, such as wide-ranging-tunable group-velocities, enhanced spatiotemporal propagating-invariance, etc., and bring new opportunities for applications.

Recently, kinds of spatiotemporal coupling methods are widely used to control the propagation and the structure of coherent light [24-45]. In our previous works, we have proposed a method to control the group-velocity and the group-acceleration of the Bessel-X optical wave-packet by separating the pulse-front from the phase-front and shaping the pulse-front from a plane into an arbitrarily-axisymmetric distribution, and in simulation superluminal or luminal or subluminal group-velocities, accelerating or uniform-motion or decelerating accelerations, and even nearly-programmable group-velocities (e.g., periodically variable group-velocity and group-acceleration in a single propagating path) have been demonstrated [46, 47]. In this paper, referring to the previous references [24-38], we studied this group-velocity-tunable Bessel-X optical wave-packet in both the physical space and the Fourier space, and systematically explained the mechanism why the group-velocity could be controlled, which would help well understand this group-velocity-tunable Bessel-X optical wave-packet and explore possible applications. We also discussed the connection with the recently-reported space-time optical wave-packet by A. Abouraddy et al. [30-37], which has freely tunable group-velocity and group-acceleration. In essence, the group-velocity-tunable Bessel-X optical wave-packet is a subsection of the space-time optical wave-packet, because, in the Fourier space, the spatiotemporal spectrum of the group-velocity-tunable Bessel-X optical wave-packet lies in that of the space-time optical wave-packet (or the spatiotemporal spectrum of the group-velocity-tunable Bessel-X optical wave-packet is a part of that of the space-time optical wave-packet), and the main difference is the spatiotemporal spectrum of the group-velocity-tunable Bessel-X optical wave-packet includes two separate short lines not a single continuous conic curve on the light-cone in the Fourier space.

Results

Group-velocity-tunable Bessel-X optical wave-packet generation. The Bessel beam can be produced by the conical superposition of plane waves, for example by using an axicon [48, 49], and the produced Bessel beam has constant superluminal phase and group velocities v_p and v_g in the vacuum [13]

$$\frac{v_p}{c} = \frac{v_g}{c} = \frac{1}{cos\theta}, \quad (1)$$

where, c is the light speed in the vacuum and θ is the half conical-angle for the conical superposition, i.e., the axicon induced propagating direction changes of plane waves with respect to the optical axis (z-axis).

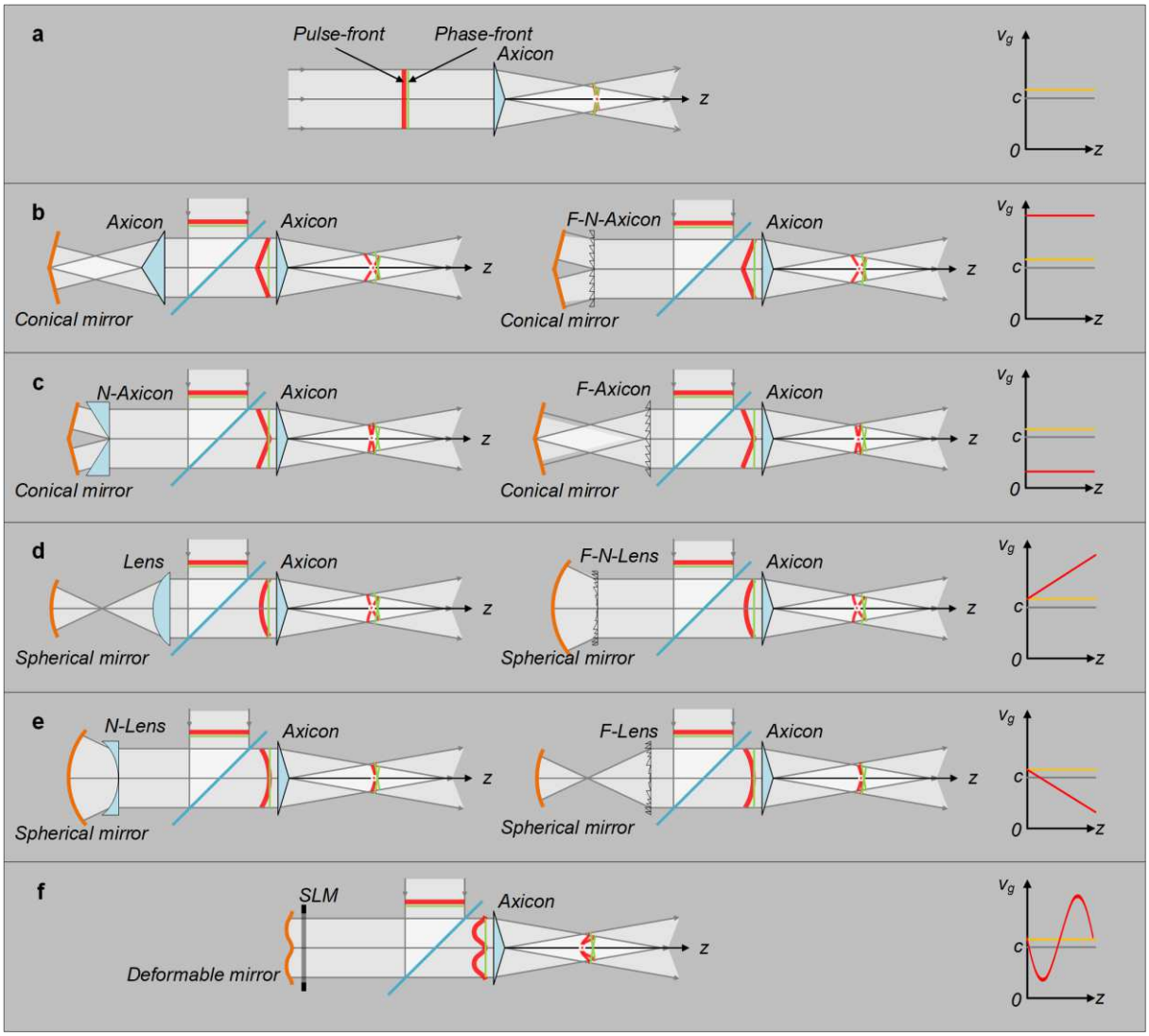

Fig. 1 Ideal thin axicon generated Bessel-X optical wave-packet for different pulse-front deformations. a Without any pulse-front deformation, Bessel-X optical wave-packet has a constant slightly-superluminal group-velocity (yellow curve), and light speed c in vacuum is given for reference (gray curve); **b** setups and generated concave-conical pulse-front deformation, Bessel-X optical wave-packet has a superluminal group-velocity (red curve); **c** setups and generated convex-conical pulse-front deformation, Bessel-X optical wave-packet has a subluminal group-velocity (red curve); **d** setups and generated concave-spherical pulse-front deformation, Bessel-X optical wave-packet has an accelerating group-velocity (red curve); **e** setups and generated convex-spherical pulse-front deformation, Bessel-X optical wave-packet has a decelerating group-velocity (red curve); and **f** setup and generated axisymmetric complex pulse-front deformation, Bessel-X optical wave-packet has a variable group-velocity. F-Axicon, Fresnel axicon; F-N-Axicon, Fresnel negative axicon; N-Axicon, negative axicon; F-Lens, Fresnel lens; F-N-Lens, Fresnel negative lens; N-Lens, negative lens; and SLM, spatial light modulator.

Figure 1a shows when all frequencies of the input pulsed beam are plane waves and overlap with one another perfectly, the pulse-front (pulse-peak across the beam aperture) overlaps with the phase-front (wave-front of the center angular frequency) perfectly, and the produced Bessel-X optical wave-packet by an ideal thin axicon has a constant slightly-superluminal group-velocity as illustrated by the yellow line in the v_g-z plot that can be well described by Eq. (1). However, when we deform the pulse-front of the input pulsed beam from a plane into an arbitrarily-axisymmetric distribution while keeping the plane phase-front unchanged, the propagation of the produced Bessel-X optical wave-packet would be changed.

We firstly discuss the axisymmetric pulse-front tilt. Figure 1b shows when the deformed pulse-front is concave-conical, the group-velocity of the produced Bessel-X optical wave-packet increases to a constant superluminal as illustrated by the red line in the v_g-z plot. The combination of an axicon and a conical mirror or that of a Fresnel negative axicon (see Fig. 2b) and a conical mirror can produce such a concave-conical pulse-front, where the conical mirror retroreflects the pulsed beam and accordingly keeps the plane phase-front unchanged and the axicon or the Fresnel negative axicon introduces bigger and smaller group delays at the beam center and edges, respectively. Figure 1c shows when the deformed pulse-front is convex-conical, the group-velocity of the produced Bessel-X optical wave-packet decreases to a constant subluminal as illustrated by the red line in the v_g-z plot. The combination of a negative axicon and a conical mirror or that of a Fresnel axicon (see Fig. 2a) and a conical mirror can produce such a convex-conical pulse-front, where the conical mirror retroreflects the pulsed beam and keeps the plane phase-front unchanged and the negative axicon or the Fresnel axicon introduces smaller and bigger group delays at the beam center and edges, respectively.

We secondly discuss the axisymmetric pulse-front curvature. Figure 1d shows when the deformed pulse-front is concave-spherical, the group-velocity of the produced Bessel-X optical wave-packet accelerates linearly from slightly-superluminal [governed by Eq. (1)] to increased-superluminal during propagation as illustrated by the red line in the v_g-z plot. The combination of a lens and a spherical mirror or that of a Fresnel negative lens [see Fig. 2d] and a spherical mirror can produce such a concave-spherical pulse-front, where the spherical mirror retroreflects the pulsed beam and keeps the plane phase-front unchanged and the lens or the Fresnel negative lens introduces bigger and smaller group delays at the beam center and edges, respectively. Figure 1e shows when the deformed pulse-front is convex-spherical, the group-velocity of the produced Bessel-X optical wave-packet decelerates linearly from slightly-superluminal [governed by Eq. (1)] to reduced-subluminal during propagation as illustrated by the red line in the v_g-z plot. The combination of a negative lens and a spherical mirror or that of a Fresnel lens (see Fig. 2c) and a spherical mirror can produce such a convex-spherical pulse-front, where the spherical mirror retroreflects the pulsed beam and keeps the plane phase-front unchanged and the negative lens or the Fresnel lens introduces smaller and bigger group delays at the beam center and edges, respectively.

We lastly discuss the axisymmetric complex pulse-front deformation. Figure 1f shows when the deformed pulse-front has an axisymmetric complex profile, e.g., axisymmetric cosine-function-like profile, the group-velocity of the produced Bessel-X optical wave-packet has a sine-function-like variation between reduced-subluminal and increased-superluminal during propagation as illustrated by the red curve in the v_g-z plot. The combination of a deformable mirror and a SLM (see Fig. 2e) can produce an arbitrarily complex pulse-front, where the deformable mirror shapes both the phase-front and the pulse-front, i.e., no deviation between them, and the SLM corrects the shaped phase-front back to a plane while keeps the shaped pulse-front unchanged [50].

In summary, when above pulse-front-deformed (plane-phase-front-unchanged) pulsed beams are injected into an ideal thin axicon for generating Bessel-X optical wave-packets, and the result is: the propagating direction of the produced Bessel-X optical wave-packet is along the z-axis and determined by the unchanged plane phase-front, while the propagation forms, including the group-velocity and the group-acceleration, are changed and dominated by the deformed axisymmetric pulse-front, which theoretically can be arbitrarily controlled.

The optical elements used to separate the pulse-front from the phase-front of a pulsed beam includes transmission optics and Fresnel elements. In transmission optics, e.g., those given in Figs. 2a-2d, the pulse-front is delayed in time with respect to the phase-front due to the difference between the group-velocity and the phase-velocity in the normal dispersion medium [51], and after collimation (plane phase-front), the deformed pulse-front has the same spatial profile as that of the transmission optics (see Figs. 1b-1e). Fresnel elements, e.g., those given in Figs. 2a-2d, can shape the phase-front like their corresponding transmission optics but almost have no influence on the pulse-front [51], i.e., separating the pulse-front from the phase-front, and after collimation (plane phase-front), the deformed pulse-front has the opposite spatial profile as that of the corresponding transmission optics (see Figs. 1b-1e). Figure 2e shows that the SLM is an arbitrarily controllable Fresnel element used to generate a complex phase-front while almost keeping the pulse-front unchanged.

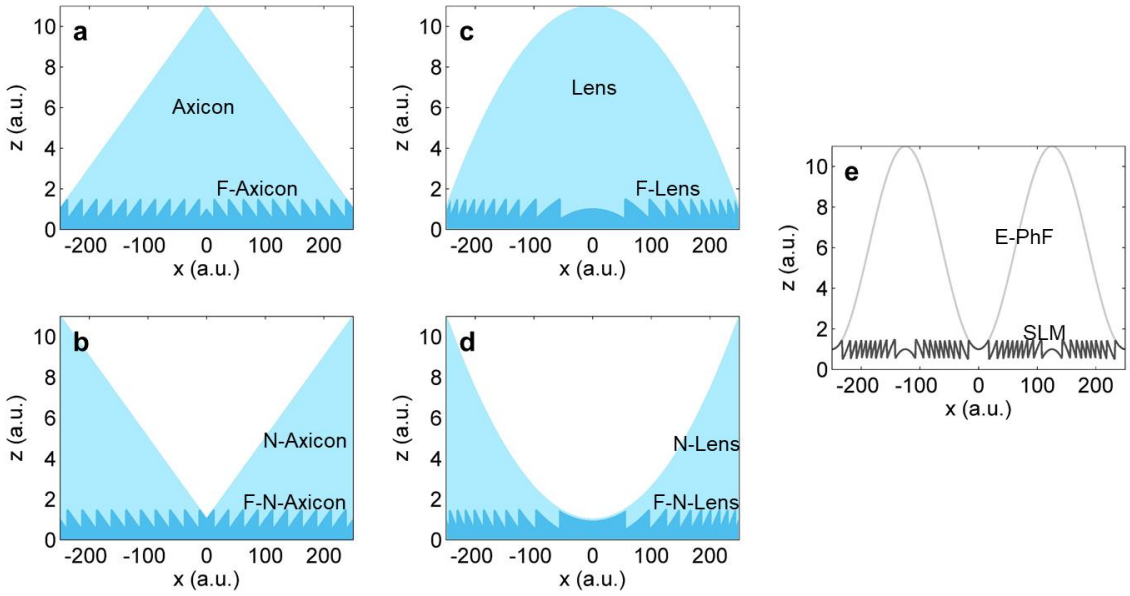

Fig. 2 Fresnel elements and SLM. a Axicon and Fresnel axicon (F-Axicon); **b** Negative axicon (N-Axicon) and Fresnel negative axicon (F-N-Axicon); **c** Lens and Fresnel lens (F-Lens); **d** Negative lens (N-Lens) and Fresnel negative lens (F-N-Lens); and **e** SLM's phase modulation and its equivalent phase-front (E-PhF). SLM, spatial light modulator.

Mechanism in the physical space. In the physical space, a monochromatic Bessel beam in the cylindrical coordinates ρ-φ-z generated by the conical superposition of a monochromatic plane wave is given by [19]

$$E_B(\rho, z, t, k, \theta) = J_0(k\rho sin\theta) exp[i(kzcos\theta - \omega t)], \qquad (2)$$

where, ρ, φ, and z are the transverse length, angle, and longitudinal length coordinates, respectively, t is the time, k is the wavenumber ($k = \omega/c$ in the vacuum), ω is the angular frequency, J_0 is the zeroth-order Bessel function of the first kind, and θ is the half conical-angle (i.e., propagating directions of plane waves with respect to the z-axis for conical superposition). Equation (2) shows both the phase and the group velocities of the Bessel beam along the z–axis are given by Eq. (1). Because the half conical-angle θ usually is only slightly larger than 0 (typically $0 < \theta < 10°$) for producing a long-distance propagating Bessel beam, the phase and the group velocities accordingly are slightly-superluminal (typically $c < v_p = v_g < 1.015c$).

Replacing the monochromatic wave by a plane pulsed beam, the Bessel beam becomes a Bessel-X beam, which can be presented as the coherent superposition of a series of monochromatic Bessel beams with different frequencies ω [26]

$$E_{BX}(\rho, z, t, \theta_0) = \int dk\, S(k) E_B(\rho, z, t, k, \theta_0), \qquad (3)$$

where, $S(k)$ is the spectral amplitude and θ_0 is a frequency-independent constant half conical-angle. Because of a frequency-independent constant half conical-angle θ_0, the phase and the group velocities of the Bessel-X optical wave-packet are still same and also given by Eq. (1). In geometrical optics, Fig. 3a shows when an ideal thin axicon is located at the ρ-plane, the propagation of only the upper half beam for the conical superposition in the lateral plane is illustrated due to the axisymmetric distribution about the z-axis. The produced Bessel-X optical wave-packet, i.e., the intersection of the pulse-front and the z-axis (group-velocity), moves along the z-axis and perfectly overlaps with the intersection of the phase-front and the z-axis (phase-velocity), that is the group and the phase velocities have no difference and are well governed by Eq. (1).

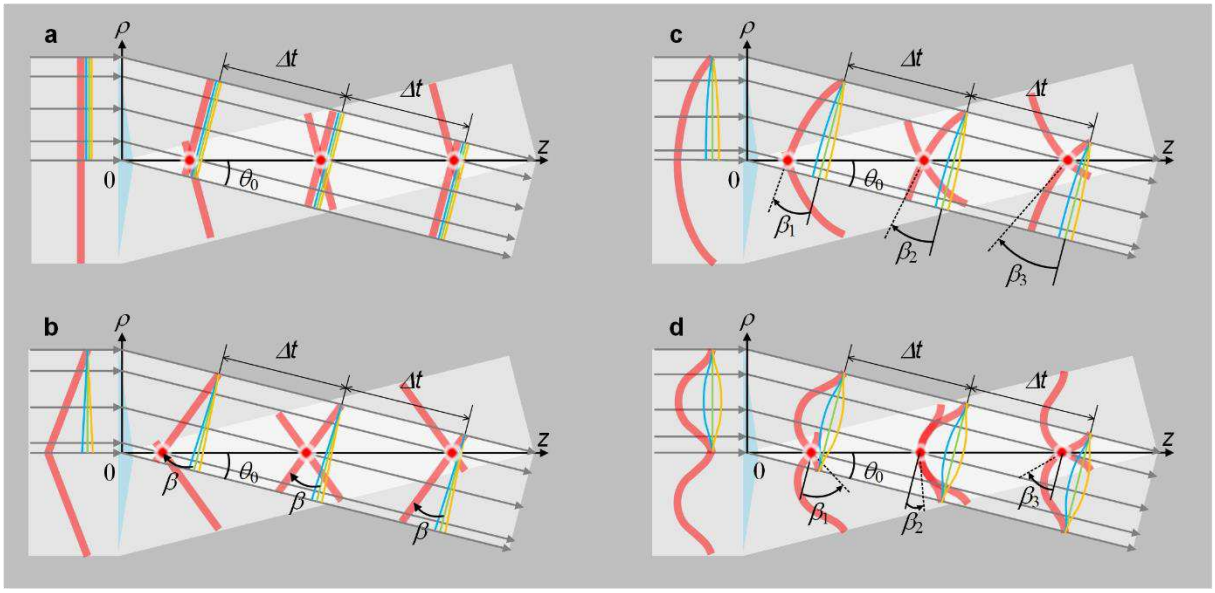

Fig. 3 Influence of pulse-front deformation of input pulsed beam on instantaneous group-velocity of produced Bessel-X optical wave-packet. Because distribution is axisymmetric about z-axis, only upper input half beam for conical superposition is illustrated. Red thick curve denotes pulse-front; blue, green and yellow curves denote wave-fronts of the highest, center and lowest frequencies, and that of center frequency is defined as phase-front; θ_0 is half conical-angle for phase-front; β is pulse-front tilt angle with respect to phase-front; and Δt is a fixed time gap during propagation. **a** Without pulse-front deformation, instantaneous group-velocity is only determined by θ_0. With pulse-front deformation, instantaneous group-velocity is determined by both θ_0 and β, and β is constant for **b** a tilted pulse-front, linearly increases for **c** a spherical pulse-front, and periodically varies for **d** a cosine-function-like pulse-front.

When the half conical-angle becomes frequency-dependent θ_ω (or wavenumber-dependent θ_k), angular dispersion appears, and the Bessel-X beam is then given by [19]

$$E_{BX}(\rho,z,t)=\int dk\int_0^{\pi} d\theta\, A(k,\theta)E_B(\rho,z,t,k,\theta), \tag{4}$$

where, $A(k,\theta)$ denotes the spatio-spectral correlation and can be presented by the Dirac function as [19]

$$A(k,\theta)=S(k)\delta(\theta-\theta_\omega). \tag{5}$$

The frequency-dependent half conical-angle (angular dispersion) would separate the pulse-front from the phase-front resulting in a pulse-front tilt angle [21, 52, 53]. We define $d\theta/d\omega$ as the conical-angle dispersion and β as the pulse-front tilt angle with respect to the phase-front, and both are axisymmetric about the z-axis and satisfy the relationship

$$tan\beta=\omega_0\frac{d\theta}{d\omega}, \tag{6}$$

where ω_0 is the center angular frequency. Figure 3b illustrates a typical case of an increased-superluminal group-velocity: within the same propagating time periods as shown in Fig. 3a, the intersection of the pulse-front and the z-axis has a longer propagating length than the intersection of the phase-front and the z-axis, the latter (phase-velocity) can still be well described by Eq. (1), while the former (group-velocity) is governed by the revised group-velocity equation [46]

$$\frac{v_g}{c}=\frac{cos\beta}{cos(\theta_0+\beta)}, \tag{7}$$

where both the half conical-angle θ_0 determined by the phase-front and the pulse-front tilt angle β dominated by the conical-angle dispersion $d\theta/d\omega$ can influence the group-velocity v_g, i.e., the pulse-front tilt angle β becomes another degree of freedom to control the group-velocity.

In this paper, we define the clockwise rotation from the wave-front of a lower frequency to that of a higher frequency (for the input upper half beam) as the positive conical-angle dispersion $d\theta/d\omega$ and the clockwise rotation from the phase-front to the pulse-front (for the input upper half beam) as the positive pulse-front tilt angle β.

Next, we consider a general form, when the pulse-front tilt angle is space-dependent across the beam aperture (but still axisymmetric about the z-axis), the group-velocity varies during propagation and can be described by

$$\frac{v_g(z)}{c} = \frac{cos\beta(\rho)}{cos[\theta_0+\beta(\rho)]}, \tag{8}$$

where, $v_g(z)$ is the variable group-velocity along the z-axis and $\beta(\rho)$ is the variable pulse-front tilt angle along the ρ-axis at the input. $\beta(\rho)$ can also be written as a variable pulse-front tilt angle $\beta(z)$ at the z-axis, and the transverse and the longitudinal coordinates satisfy the conical superposition relationship $\rho/z = \tan\theta_0$. Figure 3c illustrates when the input has a concave-spherical pulse-front deformation, from the beam center to the beam edge the pulse-front tilt angle $\beta(\rho)$ increases from zero to the maximum, and the instantaneous group-velocity $v_g(z)$ of the Bessel-X optical wave-packet (the intersection of the pulse-front and the z-axis) is increasing, showing accelerating group-velocity. Figure 3d illustrates a more complex case that the input has an axisymmetric cosine-function-like pulse-front deformation, accordingly the pulse-front tilt angle $\beta(\rho)$ varies periodically from the beam center to the beam edge, and the instantaneous group-velocity $v_g(z)$ of the Bessel-X optical wave-packet (the intersection of the pulse-front and the z-axis) also varies periodically during propagation along the z-axis, showing periodically variable (decelerating-accelerating-decelerating here) group-velocity. All of these phenomena can be approximately described by Eq. (8).

It is worth noting that here the geometrical optics approximation is considered and both diffraction and dispersion-induced distortion are neglected. When the pulse-front tilt angle $\beta(\rho)$, accordingly the conical-angle dispersion $d\theta(\rho)/d\omega$, is too large, these two factors would become too serious to destroy the propagation-invariance and break the geometrical approximation of the Bessel-X optical wave-packet.

Mechanism in the Fourier space. P. Saari et al. have studied localized (propagation-invariant) waves in the Fourier space $k_\perp$-k_z-k [26-28], where, $k_\perp$ and k_z denotes the wavevector component along the transverse and the longitudinal coordinate, respectively, and $\perp$-axis can be x- or y-axis in the Cartesian coordinates. The spatiotemporal spectrum of a propagation-invariant optical wave-packet must be the intersecting curve on the light-cone by a spectral plane parallel to the $k_\perp$-axis and its projection onto the k_z-k plane is a straight line with a slope

$$tan\alpha = \frac{v_g}{c}, \tag{9}$$

where α is the tilt angle of the spectral plane.

The spatiotemporal spectrum of a propagation-invariant optical wave-packet is solved by the simultaneous equations [32]

$$k_\perp^2 + k_z^2 = k^2, \tag{10}$$

and

$$(k - k_v) = (k_z - k_v)tan\alpha, \tag{11}$$

where, Eq. (10) is the light-cone in the vacuum, Eq. (11) is the spectral plane parallel to the $k_\perp$-axis, $k_\perp = k\cdot\sin\theta$ and $k_z = k\cdot\cos\theta$ are the transverse and longitudinal components of k, θ is the direction of k in the $k_\perp$-k_z plane (i.e., the half conical-angle in the physical space), and k_v is the wavenumber of the vertex of the spatiotemporal spectrum. Refer to Ref. [32], in Eq. (11) the vertex of the spatiotemporal spectrum is defined as the intersecting point between the spatiotemporal spectrum and the plane k_z-k (or $k_\perp = 0$) at the positive direction of the k_z-axis, and its coordinates are $(k_\perp, k_z, k) = (0, k_v, k_v)$, where $k_v > 0$. Because the spectral plane is always parallel to the $k_\perp$-axis, its tilt angle α is defined with respect to the positive direction of the k_z-axis.

A. Abouraddy et al. have used this Fourier space method to investigate their space-time optical wave-packet [30-37], and by positioning a SLM at the Fourier plane of a grating 4-f setup (pulse shaper), the spatiotemporal spectrum (including tilt angle and shape) on the light-cone intersected by the spectral plane, and accordingly the propagation characteristic, has been arbitrarily controlled.

Here, we also use this Fourier space method to study the group-velocity-tunable Bessel-X optical wave-packet for comparison with the result obtained in the physical space. By solving the simultaneous Eqs. (10) and (11), the spatiotemporal spectrum is given by

$$cos[\theta(\omega)] = \frac{\omega_v+(\omega-\omega_v)cot\alpha}{\omega}, \tag{12}$$

where ω_v is the vertex angular frequency corresponding to k_v.

Because the phase-front (the wave-front of the center angular frequency ω_0) before the ideal thin axicon is well collimated to a plane, the half conical-angle θ_0 for the center angular frequency ω_0 is fixed to constant by the ideal thin axicon, that is the spectral plane in the Fourier space must pass through a fixed straight line $(k_z, k) = (\omega_0/c\cdot\cos\theta_0, \omega_0/c)$, as illustrated by the

green thick straight line through the light-cone in Fig. 4. Then the vertex of the spatiotemporal spectrum becomes the only-one parameter determining the tilt angle α of the spectral plane. Figure 4a shows when the vertex is at the origin ($k_\perp$, k_z, k) = (0, 0, 0), Eq. (12) is simplified to $\tan\alpha = 1/\cos\theta$, the tilt angle α of the spectral plane in the Fourier space is directly linked with the half conical-angle θ in the physical space, and θ is constant without any angular dispersion $d\theta/d\omega = 0$ (see angular dispersion in the $\perp$-z plane in the physical space and wavevectors in the $k_\perp$-k_z plane in the Fourier space). Figure 4a also gives the projection of the spatiotemporal spectrum in the k_z-k plane: ω_l, ω_0, ω_h are the lowest, center and highest angular frequencies of the pulse; and the spatiotemporal spectrum projection is a straight line through the fixed point (k_z, k) = ($\omega_0/c\cdot\cos\theta_0$, ω_0/c) and the vertex (k_z, k) = (0, 0), that is the tilt angle α is determined by both the fixed point and the vertex. If the vertex of the spatiotemporal spectrum is not at the origin, Fig. 4b shows when the spectral plane is rotated counterclockwise about the fixed straight line (k_z, k) = ($\omega_0/c\cdot\cos\theta_0$, ω_0/c) to increase the tilt angle α of the spectral plane and accordingly to increase the group-velocity v_g of the Bessel-X optical wave-packet, positive conical-angle dispersion $d\theta/d\omega > 0$ appears (see angular dispersion in the $\perp$-z plane in the physical space and wavevectors in the $k_\perp$-k_z plane in the Fourier space). Similarly, Fig. 4c shows when the spectral plane is rotated clockwise about the fixed straight line (k_z, k) = ($\omega_0/c\cdot\cos\theta_0$, ω_0/c) to reduce the tilt angle α of the spectral plane and accordingly to reduce the group-velocity v_g of the Bessel-X optical wave-packet, negative conical-angle dispersion $d\theta/d\omega < 0$ appears (see angular dispersion in the $\perp$-z plane in the physical space and wavevectors in the $k_\perp$-k_z plane in the Fourier space).

By differentiating two sides of Eq. (12) about the center angular frequency ω_0, the conical-angle dispersion is given by

$$\frac{d\theta}{d\omega} = \frac{(1-cot\alpha)}{sin\theta_0}\frac{\omega_v}{\omega_0^2}. \tag{13}$$

From Eq. (12), the vertex angular frequency ω_v can be described by

$$\omega_v = \frac{\omega_0(cos\theta_0 - cot\alpha)}{1-cot\alpha}. \tag{14}$$

By the substitution of Eq. (13) with Eq. (14), we have

$$tan\alpha = \frac{1}{cos\theta_0 - \omega_0\frac{d\theta}{d\omega}sin\theta_0}. \tag{15}$$

Equation (15) shows the tilt angle α of the spectral plane can be changed by introducing and then adjusting a non-zero conical-angle dispersion $d\theta/d\omega$. Equations (15) and (9) link the conical-angle dispersion $d\theta/d\omega$ with the tilt angle α of the spectral plane and accordingly with the group-velocity v_g of the Bessel-X optical wave-packet. Because the half conical-angle θ_0 usually is very small, the tilt angle α, and accordingly the group-velocity v_g, increases with increasing the conical-angle dispersion $d\theta/d\omega$, and vice versa.

When the conical-angle dispersion is not constant and becomes space-dependent across the beam aperture $d\theta(\perp)/d\omega$ (but still axisymmetric about the z-axis), the tilt angle $\alpha(z)$ of an instantaneous spectral plane in the Fourier space, which corresponds to an instantaneous Bessel-X optical wave-packet propagating at the z-axis in the physical space, should be revised as

$$tan\alpha(z) = \frac{1}{cos\theta_0 - \omega_0\frac{d\theta(\perp)}{d\omega}sin\theta_0}, \tag{16}$$

where, $d\theta(\perp)/d\omega$ is the variable conical-angle dispersion along the $\perp$-axis at the input, and the transverse and longitudinal coordinates satisfy the conical superposition relationship $\perp/z = \tan\theta_0$. Figure 4d illustrates when the input has a concave-spherical pulse-front deformation, from the beam center to the upper beam edge the conical-angle dispersion $d\theta(\perp)/d\omega$ increases linearly from zero to the maximum, and the corresponding tilt angle $\alpha(z)$ of the spectral plane in the Fourier space is rotated counterclockwise from with the tilt angle α_1 to with the tilt angle α_2. Here, α_1 is smaller than α_2, which corresponds to the conical-angle dispersion at the beam center $d\theta(0)/d\omega$ and at the beam upper edge $d\theta(r)/d\omega$, respectively, showing accelerating group-velocity. Figure 4e illustrates when the input has an axisymmetric cosine-function-like pulse-front deformation, from the beam center to the upper beam edge the conical-angle dispersion $d\theta(\perp)/d\omega$ decreases from zero to the minimum, increases to zero and then maximum, and finally decreases to zero again, and the corresponding tilt angle $\alpha(z)$ of the spectral plane in the Fourier space is rotated clockwise from with the tilt angle α_1 to with the tilt angle α_2, counterclockwise to with the tilt angle α_1 and then α_3, and finally clockwise to with the tilt angle α_1 again. Here, the three tilt angles have the relationship $\alpha_2 < \alpha_1 < \alpha_3$, which corresponds to the smallest, zero, and largest conical-angle dispersion $d\theta(\perp)/d\omega$ across the input beam aperture, respectively, showing periodically variable (decelerating-accelerating-decelerating here) group-velocity. If neglecting the diffraction distortion, the variation of the tilt angle $\alpha(z)$ of the spectral plane in the Fourier space, which corresponds to a propagating Bessel-X optical wave-packet, can be described by Eq. (16). However, if the

conical-angle dispersion $d\theta(\perp)/d\omega$ is too large, the geometrical approximation is destroyed by propagation diffraction and dispersion-induced distortion, and the Bessel-X optical wave-packet would disappear during propagation [47].

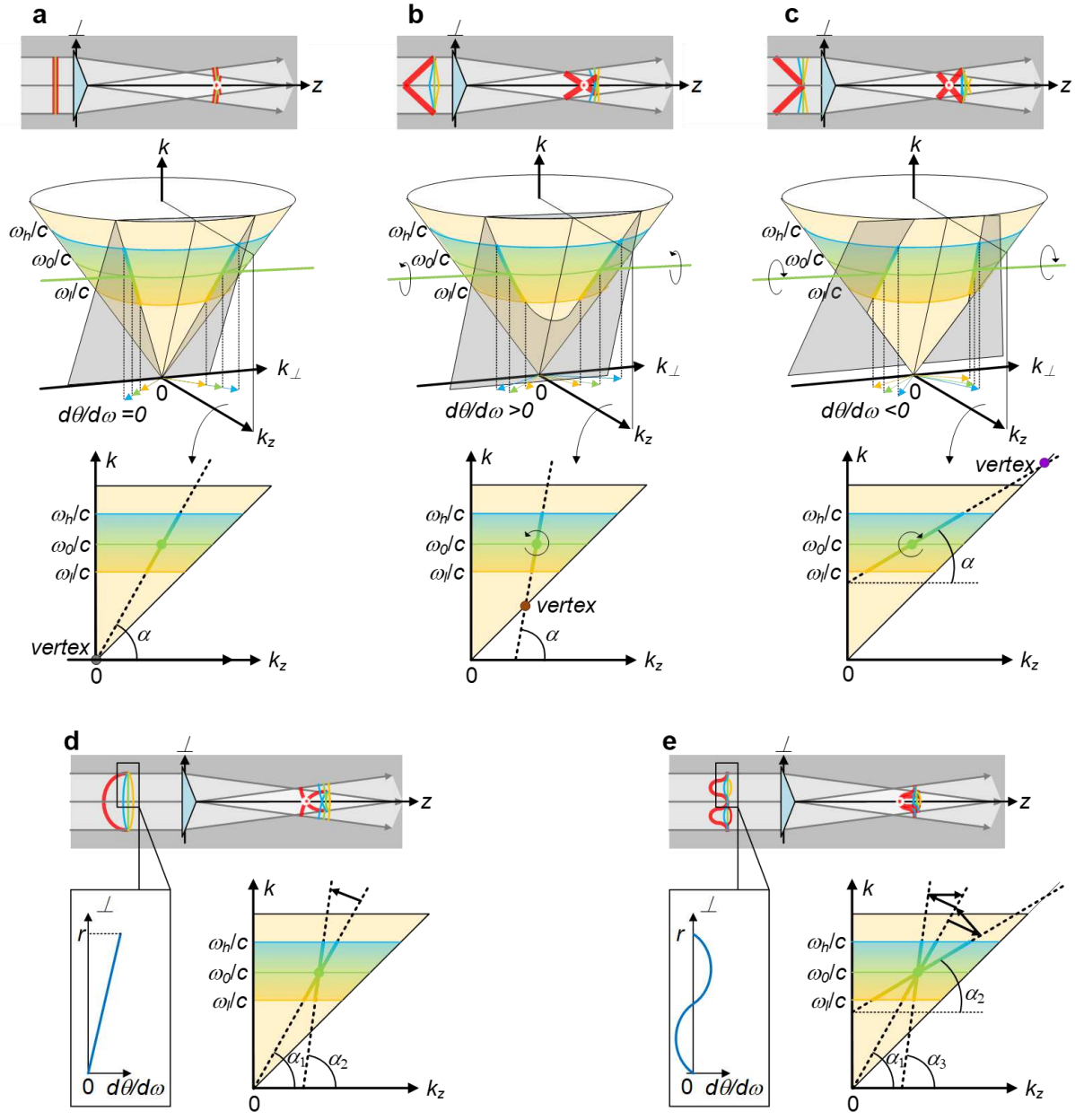

Fig. 4 Group-velocity-tunable Bessel-X optical wave-packet and its spatiotemporal spectrum in the Fourier space. Spatiotemporal spectrum (colored thick line) of Bessel-X optical wave-packet is a part of intersecting curve between light-cone and spectral plane, and spectral plane is parallel to $k_\perp$-axis and passes through green thick straight line (k_z, k) = ($\omega_0/c\cdot\cos\theta_0$, ω_0/c). Vertex is defined as intersecting point between spatiotemporal spectrum's locus and plane $k_\perp = 0$ at positive direction of k_z-axis. **a** Without angular dispersion $d\theta/d\omega = 0$, vertex is at origin; **b** with positive angular dispersion $d\theta/d\omega > 0$, vertex is $k_v < \omega_l/c$, and spectral plane is rotated counterclockwise about line (k_z, k) = ($\omega_0/c\cdot\cos\theta_0$, ω_0/c); **c** with negative angular dispersion $d\theta/d\omega < 0$, vertex is $k_v > \omega_h/c$, and spectral plane is rotated clockwise about line (k_z, k) = ($\omega_0/c\cdot\cos\theta_0$, ω_0/c); **d** with concave-spherical pulse-front deformation, at input from beam center to upper beam edge, angular dispersion $d\theta/d\omega$ increases linearly from zero to maximum, and corresponding spectral plane in the Fourier space gradually rotates counterclockwise from tilt angle α_1 to α_2 ($\alpha_1 < \alpha_2$); and **e** with cosine-function-like pulse-front deformation, at input from beam center to upper beam edge, angular dispersion $d\theta/d\omega$ decreases from zero to minimum, increases to zero and then

maximum, and decreases to zero eventually, and corresponding spectral plane in the Fourier space gradually rotates clockwise from tilt angle α_1 to α_2, counterclockwise to α_1 and then α_3, and clockwise to α_1 eventually ($\alpha_2 < \alpha_1 < \alpha_3$). k_v is wavenumber of vertex, ω_l, ω_0, and ω_h are the lowest, center and highest angular frequencies of pulse, and r is beam radius.

Extension and discussion

In the physical space, the tunable group-velocity v_g of the Bessel-X optical wave-packet is due to the pulse-front tilt angle β, which is caused by the conical-angle dispersion $d\theta/d\omega$. In the Fourier space, the tunable group-velocity v_g of the Bessel-X optical wave-packet is due to the tilt angle α of the spectral plane, which is also caused by the conical-angle dispersion $d\theta/d\omega$. If substituting Eq. (15) with Eq. (6), Eq. (15) becomes Eq. (7), which shows the group-velocity equation derived in the Fourier space and that derived in the physical space are exactly equivalent. Then, the nature of controlling the group-velocity of the Bessel-X optical wave-packet is introducing and then adjusting the conical-angle dispersion across the input beam aperture. It is worth mentioning that the conical-angle dispersion should be axisymmetric about the z-axis for producing a straight-line propagating Bessel-X optical wave-packet.

Figure 5 shows, in the Fourier space, the spatiotemporal spectrum of the Bessel-X optical wave-packet consists of two separate lines (two parts of the conic curve and excluding $k_\perp = 0$) lying in the intersecting curve between the light-cone and the spectral plane parallel to the $k_\perp$-axis, which are symmetric about the k-k_z plane. The spatiotemporal spectrum of the space-time optical wave-packet, well studied by A. Abouraddy et al. [30-37], is a single continuous conic curve (including $k_\perp = 0$) lying in the intersecting curve between the light-cone and the spectral plane parallel to the $k_\perp$-axis. In this case, the group-velocity-tunable Bessel-X optical wave-packet should be a subsection of the space-time optical wave-packet.

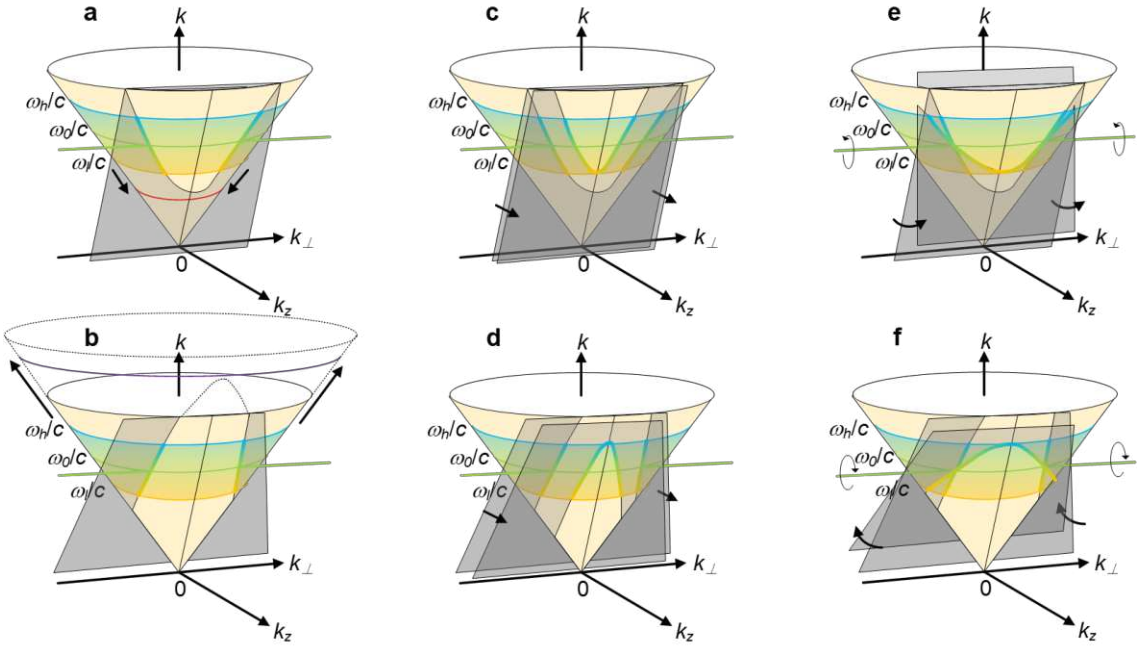

Fig. 5 Group-velocity-tunable Bessel-X optical wave-packet is subsection of space-time optical wave-packet. Spatiotemporal spectrum (colored thick line on light-cone) of Bessel-X optical wave-packet is a part of that of space-time optical wave-packet, excluding $k_\perp = 0$. When **a b** spectral range of pulse is enhanced, or spectral plane is **c d** shifted towards positive direction of k_z-axis, or spectral plane is rotated **e** counterclockwise or **f** clockwise, spatiotemporal spectrum of Bessel-X optical wave-packet is changed from two separate curves about $k_\perp = 0$ plane into a single continuous one, and Bessel-X optical wave-packet becomes space-time optical wave-packet. ω_l, ω_0, and ω_h are the lowest, center and highest angular frequencies of pulse.

Figures 5a and 5b show if we can significantly increase the spectral range of the pulse, especially the lowest angular frequency ω_l and the highest angular frequency ω_h for the case of the increased (superluminal) and the reduced (subluminal) group-velocity, respectively, and also optimize the introduced conical-angle dispersion, the spatiotemporal spectrum can be changed from two separate lines into a single continuous conic curve, and the Bessel-X optical wave-packet would be

improved to the space-time optical wave-packet. Besides, Figs. 5c and 5d show, no matter for the case of the group-velocity increased (superluminal) or reduced (subluminal) Bessel-X optical wave-packet, we can shift the spectral plane towards the positive direction of the k_z-axis to make the spatiotemporal spectrum continuous within the spectral range of the pulse by dramatically reducing the conical angle generated by the thin axicon and also modifying the introduced conical-angle dispersion. In addition, Figs. 5e and 5f show we can also significantly rotate the spectral plane about the fixed straight line $(k_z, k) = (\omega_0/c \cdot \cos\theta_0, \omega_0/c)$ counterclockwise and clockwise for the case of the group-velocity increased (superluminal) and reduced (subluminal) Bessel-X optical wave-packet, respectively, to produce a continuous spatiotemporal spectrum within the spectral range of the pulse by significantly increasing the absolute value and also modifying the introduced conical-angle dispersion. In the above processes of changing the spatiotemporal spectrum from two separate lines into a single continuous conic curve, the classic optics we used in Fig. 1 are not enough, and elements like SLM, just as Abouraddy et al. have done, are necessary.

Conclusion

In conclusion, we have systematically introduced the group-velocity-tunable Bessel-X optical wave-packet. The classic optical setups for generating Bessel-X optical wave-packets with superluminal, subluminal, accelerating, decelerating, and near-programmable periodically-variable group-velocities are introduced. The mechanism of the tunability of the group-velocity is analyzed in the physical space and the Fourier space, respectively, and the group-velocity equations are derived in two spaces and also linked in mathematics. In the physical space, the Bessel-X optical wave-packet is generated by the conical superposition of pulse-fronts. The Bessel-X optical wave-packets at different propagating locations have different instantaneous pulse-front tilt angles and accordingly have different instantaneous group-velocities. While, in the Fourier space, the spatiotemporal spectrum of the Bessel-X optical wave-packet lies in the intersecting curve between the light-cone and a spectral plane parallel to the $k_\perp$-axis, and the tilt angle of the spectral plane determines the group-velocity. The Bessel-X optical wave-packets at different propagating locations correspond to different spectral planes with different tilt angles and then have different instantaneous group-velocities. However, both the pulse-front tilt angle in the physical space and the spectral plane tilt angle in the Fourier space are due to the angular dispersion, which actually is the nature of controlling the group-velocity of the Bessel-X optical wave-packet.

In the Fourier space, because the spatiotemporal spectrum of the group-velocity-tunable Bessel-X optical wave-packet lies in that of the space-time optical wave-packet, i.e., the intersecting curve between the light-cone and a spectral plane parallel to the $k_\perp$-axis, the group-velocity-tunable Bessel-X optical wave-packet is a subsection of the space-time optical wave-packet. Due to the generation methods, the spatiotemporal spectrum of the group-velocity-tunable Bessel-X optical wave-packet only consists of two separate and symmetric short lines. When increasing the spectral range of the pulse, or shifting the spectral plane in the Fourier space by reducing the conical angle, or rotating the spectral plane in the Fourier space by increasing the absolute value of the angular dispersion, the spatiotemporal spectrum would be changed from two separate lines into a single continuous conic curve, and accordingly the group-velocity-tunable Bessel-X optical wave-packet can be improved to the space-time optical wave-packet.

Data availability

All data and models generated or used during the study appear in the submitted article.

References

1. Hau, L. V., Harris, S. E., Dutton, Z. & Behroozi, C. Light speed reduction to 17 m per second in an ultracold atomic gas. Nature **397**, 594–598 (1999).
2. Wang, L. J., Kuzmich, A. & Dogariu, A. Gain-assisted superluminal light propagation. Nature **406**, 277–279 (2000).
3. Dolling, G., Enkrich, C., Wegener, M., Soukoulis, C. M. & Linden, S. Simultaneous negative phase and group velocity of light in a metamaterial. Science **312**, 892–894 (2005).
4. Gehring, G. M., Schweinsberg, A., Barsi, C., Kostinski, N. & Boyd, R. W. Observation of backward pulse propagation through a medium with a negative group velocity. Science **312**, 895–897 (2005).
5. R. W. Boyd and D. J. Gauthier, "Controlling the velocity of light pulses," Science **326**, 1074–1077 (2009).
6. Giovannini, D. et al. Spatially structured photons that travel in free space slower than the speed of light. Science **347**, 857-860 (2015).
7. Durnin, J. Exact solutions for nondiffracting beams. I. The scalar theory. J. Opt. Soc. Am. A **4**, 651-654 (1987).
8. Durnin, J., Miceli, J. J. & Eberly, J. H. Diffraction-free beams. Phys. Rev. Lett. **58**, 1499–1501 (1987).
9. Gori, F. & Guattari, G. Bessel-Gauss beams. Opt. Commun. **64**, 491-495 (1987).
10. Mcgloin, D. & Dholakia, K. Bessel beams: diffraction in a new light. Contemp. Phys. **46**, 15–28 (2005).
11. Aiello, A. & Agarwal, G. S. Wave-optics description of self-healing mechanism in Bessel beams. Opt. Lett. **39**, 6819-6822 (2014).
12. Vetter, C. et al. Realization of free-space long-distance self-healing Bessel beams. Laser Photonics Rev. **13**, 1900103 (2019).
13. Alexeev, I., Kim, K. Y. & Milchberg, H. M. Measurement of the superluminal group velocity of an ultrashort Bessel beam pulse. Phys. Rev. Lett. **88**, 073901 (2002).
14. Duocastella, M. & Arnold, C. B. Bessel and annular beams for materials processing. Laser Photonics Rev. **6**, 607-621 (2012).
15. Lu, J. & Greenleaf, J. F. Nondiffracting X waves-exact solutions to free-space scalar wave equation and their finite aperture realizations. EEE Trans. Ultrason. Ferroelectr. Freq. Control **39**, 19-31 (1992).
16. Lu, J. & Greenleaf, J. F. Experimental verification of nondiffracting X waves. IEEE Trans. Ultrason. Ferroelectr. Freq. Control **39**, 441-446 (1992).

17. Saari, P. & Reivelt, K. Evidence of X-Shaped Propagation-Invariant Localized Light Waves. Phys. Rev. Lett. **79**, 4135-4136 (1997).
18. Brittingham, J. N. Focus waves modes in homogeneous Maxwell's equations: Transverse electric mode. J. Appl. Phys. **54**, 1179 (1983).
19. Reivelt, K. & Saari, P. Optical generation of focus wave modes. J. Opt. Soc. Am. A **17**, 1785-1790 (2000).
20. Sheppard, C. J. R. Bessel pulse beams and focus wave modes. J. Opt. Soc. Am. A **18**, 2594-2600 (2001).
21. Reivelt, K. & Saari, P. Experimental demonstration of realizability of optical focus wave modes. Phys. Rev. E **66**, 056611 (2002).
22. Wang, H., Shi, L., Lukyanchuk, B., Sheppard, C. & Chong, Ch. T. Creation of a needle of longitudinally polarized light in vacuum using binary optics. Nat. Photon. **2**, 501-505 (2008).
23. Chong, A., Renninger, W. H., Christodoulides, D. N. & Wise, F. W. Airy–Bessel wave packets as versatile linear light bullets. Nat. Photon. **4**, 103–106 (2010).
24. Fagerholm, J. Friberg, A. T., Huttunen, J., Morgan, D. P. & Salomaa, M. M. Angular-spectrum representation of nondiffracting X waves. Phys. Rev. E **54**, 4347-4352 (1996).
25. Reivelt, K. & Saari, P. Optically realizable localized wave solutions of the homogeneous scalar wave equation. Phys. Rev. E **65**, 046622 (2002).
26. Saari, P. & Reivelt, K. Generation and classification of localized waves by Lorentz transformations in Fourier space. Phys. Rev. E **69**, 036612 (2004).
27. Reivelt, K., Valtna, H. & Saari, P. Optical generation of superluminal localized wave solutions of homogeneous wave equation. presented at 2006 Northern Optics, 14-16 June 2006, Bergen, Norway, DOI:10.1109/NO.2006.348365.
28. Valtna, H., Reivelt, K. & Saari, P. Methods for generating wideband localized waves of superluminal group velocity. Opt. Commun. **278**, 1-7 (2007).
29. Parker, K. J. & Alonso, M. A. Longitudinal iso-phase condition and needle pulses. Opt. Express **24**, 28669-28677 (2016).
30. Kondakci, H. E. & Abouraddy, A. F. Diffraction-free pulsed optical beams via space-time correlations. Opt. Express **24**, 28659-28668 (2016).
31. Kondakci, H. E. & Abouraddy, A. F. Diffraction-free space–time light sheets. Nat. Photon. **11**, 733-740 (2017).
32. Yessenov, M., Bhaduri, B., Kondakci, H. E. & Abouraddy, A. F. Classification of propagation-invariant space-time wave packets in free space: Theory and experiments. Phys. Rev. A **99**, 023856 (2019).
33. Kondakci, H. E. & Abouraddy, A. F. Optical space-time wave packets having arbitrary group velocities in free space. Nat. Commun. **10**, 929 (2019).
34. Bhaduri, B., Yessenov, M. & Abouraddy, A. F. Anomalous refraction of optical spacetime wave packets. Nat. Photon. **14**, 416–421 (2020).
35. Hall, L. A., Yessenov, M. & Abouraddy, A. F. Space–time wave packets violate the universal relationship between angular dispersion and pulse-front tilt. Opt. Lett. **46**, 1672-1675 (2021).
36. Hall, L. A., Yessenov, M. & Abouraddy, A. F. Arbitrarily accelerating space-time wave packets. Opt. Lett. **47**, 694-697 (2022).
37. Yessenov, M. et al. Space-time wave packets localized in all dimensions. arXiv:2111.03095, DOI:10.48550/arXiv.2111.03095.
38. Porras, M. A. Nature, diffraction-free propagation via space-time correlations, and nonlinear generation of time-diffracting light beams. Phys. Rev. A **97**, 063803 (2018).
39. Sainte-Marie, A., Gobert, O. & Quéré, F. Controlling the velocity of ultrashortlight pulses in vacuum through spatio-temporal couplings. Optica **4**,1298–1304 (2017).
40. Froula, D. H. et al. Spatiotemporal control of laser intensity. Nat. Photon. **12**, 262–265 (2018).
41. Hancock, S. W., Zahedpour, S., Goffin, A. & Milchberg, H. M. Free-space propagation of spatiotemporal optical vortices. Optica **6**, 1547-1553 (2019).
42. Simpson, T. T. et al. Nonlinear spatiotemporal control of laser intensity. Opt. Express **28**, 38516–38526 (2020).
43. Chong, A., Wan, C., Chen, J. & Zhan, Q. Generation of spatiotemporal optical vortices with controllable transverse orbital angular momentum. Nat. Photon. **14**, 350-354 (2020).
44. Li, Z., Gu, Y. & Kawanaka, J. Reciprocating propagation of laser pulse intensity in free space. Commun. Phys. **4**, 89 (2021).
45. Cao, Q. et al. Sculpturing spatiotemporal wavepackets with chirped pulses. Photon. Res. **9**, 2261-2264 (2021).
46. Li, Z. & Kawanaka, J. Velocity and acceleration freely tunable straight-line propagation light bullet. Sci. Rep. **10**, 11481 (2020).
47. Li, Z. & Kawanaka, J. Optical wave-packet with nearly-programmable group velocities. Commun. Phys. **3**, 211 (2020).
48. Indebetouw, G. Nondiffracting optical fields: some remarks on their analysis and synthesis. J. Opt. Soc. Am. A **6**, 150-152 (1989).
49. Herman, R. M. & Wiggins, T. A. Production and uses of diffractionless beams. J. Opt. Soc. Am. A **8**, 932-942 (1991).
50. Sun, B., Salter, P. S. & Booth, M. J. Pulse front adaptive optics: a new method for control of ultrashort laser pulses. Opt. Express **23**, 19348-19357 (2015).
51. Bor, Z. Distortion of femtosecond laser pulses in lenses. Opt. Lett. **14**, 119-121 (1989).
52. Bor, Z., Rácz, B., Szabó, G., Hilbert, M. & Hazim, H. A. Femtosecond pulse front tilt caused by angular dispersion. Opt. Eng. **32**, 2501–2504 (1993).
53. Li, Z. & Kawanaka, J. Efficient method for determining pulse-front distortion in an ultra-intense laser. J. Opt. Soc. Am. B **37**, 2595-2603 (2020).

Acknowledgments
This work was supported by 2049 funding at Zhangjiang Laboratory.

Author contributions
Z.L. derived the equations, carried out the analysis and prepared the manuscript. Y.Q.L., Y.X.L. & R.L. contributed to the analysis. All authors discussed the results and commented on the manuscript.

Competing interests
The authors declare no competing interests.

Correspondence and requests for materials should be addressed to Z.L.